ADVANCED MATERIALS INTERFACES
Open Access
www.advmatinterfaces.de

An Artificial Compartmentalized Biocatalytic Cascade System Constructed With Enzyme-Caged Reticulate Nanoporous Membranes

*Wangsuk Oh, Dawoon Jeong, and Ji-Woong Park**

Compartmentalization is a ubiquitous feature of life, with a membrane interface that regulates molecular transport and exhibits bioactivities. An artificial enzyme-integrated membrane cascade system can mimic such interactive properties across different length scales for in vitro application. Here, it is shown that a reticulated nanoporous framework membrane with nano-caged enzymes presents the first modular macroscale platform for the compartmentalized biocatalytic system interfaced with an external medium. Catalase (CAT)-integrated polyurea membrane scaffold is prepared by a simple pressurization procedure for a model cyclic cascade of glucose oxidase/catalase (GO*x*/CAT). The bicontinuous nanoporous membrane readily constructs a compartmentalized system interfacing the glucose/GO*x* solution and the external environment and mediates glucose oxidation by a cascade reaction under anaerobic or aerobic conditions. Furthermore, the membrane compartment exhibits multiple bioactive capabilities and barrier properties, including hydrogen peroxide detoxification, in situ oxygen generation, and protease exclusion. This work suggests a new strategy toward a robust modular biocatalytic membranous interface to mediate biochemical reaction cascades occurring in a compartment interfaced to an external environment, promising for potential applications in biohybrid devices embedded with tissues and cells.

1. Introduction

Homeostasis, a self-regulating process to maintain the integrity of a system, is a common feature of living organisms interacting with the environment.[1] Compartmentalization by a physical barrier (e.g., skin tissue[2] and cell membrane[3]) is vital for the homeostatic regulation of internal conditions such as temperature, pH, and concentration. The membranes are often integrated with functional proteins and enzymes, which selectively transport nutrients,[4] sense environmental cues,[5,6] and perform biochemical reactions at the interface.[7] For example, the crystalline bacterial cell surface layer (S-layer) provides protection and molecular sieving functions.[4,8] Cascades of enzymatic reactions[9,10] and feedback loops[11] mediated by the membrane-integrated enzymes are at the center of the regulatory functions.

Artificial membranous compartments have been extensively investigated with enzyme-incorporated supramolecular assemblies to mimic the structure of a cell[3,10,12–14] and to develop advanced biohybrid devices.[15–22] Localization of enzymes (or proteins) within the membrane allows concerted biochemical reactions for self-regulation,[13,23,24] interacting with the enzymes encapsulated in the inner/outer compartments. While nano-/micron-scale colloidal structures are common,[3,25–29] flat-sheet type structures are ideal for studying in vitro biophysical behaviors[30,31] and preparing macroscale devices interfacing large area (e.g., sensors).[32,33] However, quantitative protein reconstitution within the membrane required elaborate conditions,[23,24] and large-scale production without defect was challenging. Solid support also limits multifaceted reaction cascades that are common in nature.

Here, we demonstrate constructing a macroscale artificial compartmentalized cascade system with an enzyme-caged nanoporous membrane that separates the internal and external medium while efficiently transporting molecules. The membrane consists of a nanoporous covalent framework (NCF) of the urea-linked networks containing 3D continuous nanochannels with a pore size of ≈5–30 nm.[34–37] The bottlenecks within the continuous pore structure act as an entropic trap for the enzymes incorporated by pressurized flow, and the pore surface grafted with poly(ethylene glycol) (PEG) provides benign environments for their activity.[38–40] The facile flow-through entrapment into the membrane allows quantitative enzyme incorporation[38,41] without additional layers to prevent enzyme leaching or ensure mechanical stability.[42,43]

We envisioned that the enzyme-caged NCF membrane is suitable for building an artificial compartmentalized cascade

W. Oh, D. Jeong, J.-W. Park
School of Materials Science and Engineering
Gwangju Institute of Science and Technology
123 Cheomdangwagiro, Bukgu, Gwangju 61005, South Korea
E-mail: jiwoong@gist.ac.kr

The ORCID identification number(s) for the author(s) of this article can be found under https://doi.org/10.1002/admi.202300185.

DOI: 10.1002/admi.202300185

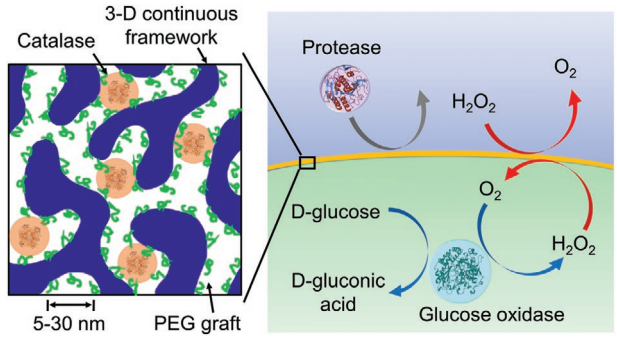

Figure 1. An artificial membrane cascade system constructed from a catalase-caged nanoporous membrane. The bicontinuous nanoporous framework allows stable catalase incorporation into the membrane through which molecules can transport in a size-selective manner. A model cascade of glucose oxidase/catalase exhibits self-regulatory functions in the compartment enclosed by the membrane.

system (**Figure 1**) in which the membranous shell performs protection and biochemical self-regulation between the outside and inside of the compartment, while the open pore structure through the membrane enables controlled solute passage via a size-sieving mechanism, readily mimicking the function of the S-layer (pore size ≈2–8 nm).[4] We employed catalase (CAT) because its molecular dimension (9.7 nm × 9.2 nm × 6.7 nm)[44] is close to the pore size of NCF, and it can decompose hydrogen peroxide and generate oxygen for the regulation of oxidase activity in the CAT/oxidase cascades. First, CAT was infiltrated into the nanopores of NCF by a pressurized permeation method, and the stability of the CAT-dispersed NCF (CAT@NCF) was evaluated under various conditions. Then, a reaction system with glucose oxidase (GO*x*) was compartmentalized in the CAT@NCF. The compartmentalized space took advantage of multiple activities of the CAT@NCF, including hydrogen peroxide detoxification, in situ oxygen generation, and protease exclusion.

2. Results and Discussion

The NCF membrane was prepared by the previously reported procedure[35] with the details given in the Supporting Information (Figure S1, Supporting Information). In brief, the urea-bonded network (UN) sol (prepared by crosslinking polymerization of tetrakis(4-aminophenyl) methane and hexamethylene diisocyanate) was mixed with PEG, which functions as a polymeric porogen and in situ grafting agent. Bicontinuous nanostructure was generated by phase separation of the PEG/UN mixture upon solvent evaporation.[35,45] Extraction of the PEG with water produced an ≈40–50 µm-thick, free-standing NCF film with a bicontinuous nanoporous structure composed of a UN skeleton and the pore wall tethered with PEG (Figures S2 and S3a and Table S1, Supporting Information). Electron microscopy and porosity measurement confirmed the pore structure of the NCF (Figure S3b–d, Supporting Information). The pore size was distributed over ≈5–30 nm, and the water flux through the membrane confirmed the open pore structure. (Figure S4, Supporting Information).

CAT was immobilized by permeating its solution through the NCF membrane under constant nitrogen gas pressure (**Figure 2**). The solution flux decreased over time because of entrapment of CAT in the nanopores. Notably, the immobilized amount of CAT in the NCF could be adjusted by simply changing the permeation time until reaching the saturation regime near 32 h, as shown in Figure 2b; Table S2, Supporting Information (The detailed quantification procedure is given in the Supporting Information). The typical immobilization time was set as 24 h, and the total amount of immobilized CAT was estimated to be 76.7 mg g^{-1} membrane, which is pretty high considering the porosity (≈0.3) of the NCF membrane.[46,47] The total pore volume decreased from 0.3 to 0.12 cm^3 g^{-1}, and the pore size distribution of CAT@NCF showed little porosity in the higher pore size range of NCF (Figure 2c; Table S3, Supporting Information). These data suggest that the enzymes occupied the larger pores, reducing their effective pore sizes. Scanning electron microscopy-energy dispersive X-ray analysis (SEM-EDX) elemental mapping of sulfur and iron (in the heme group of CAT) within NCF and CAT@NCF supports that CAT was evenly distributed over the whole membrane thickness (Figure 2d; Figure S6, Supporting Information). Although CAT loading reduced the pore size, the open and continuous nanopore structure remained similar to the original structure, as shown by the cross-sectional SEM image (Figure 2e). The embedding of CAT was also supported by the Fourier-transform infrared spectroscopy (FTIR) spectra, which included the peaks at ≈1611–1615 cm^{-1} (intermolecular β-sheets, amide I bands) and 1568 cm^{-1} (amide II band) (Figure S7, Supporting Information).[48,49]

The CAT@NCF membrane could be shaped by simple cutting and rolling, which is beneficial for customizing the bioactive film in various shapes (Figure S9, Supporting Information). We employed a circular membrane shape to study the flow mode catalysis in a cylindrical membrane cell. For a batch mode reaction, the same membrane was suspended in the reaction medium with stirring. The catalyst amount could be varied simply by cutting the membrane into different diameters or using a different number of sheets.

The catalytic performance of a CAT@NCF film was first studied by batch mode reaction of hydrogen peroxide decomposition. CAT@NCF sheets decomposed hydrogen peroxide for several hours, whereas a control NCF film (without CAT) displayed no activity (**Figure 3**a). A CAT@NCF prepared with a larger dimension showed a higher decomposition rate, and the activity normalized by the membrane area was nearly identical for the two membranes (Figure S10a, Supporting Information). Furthermore, the activity increased linearly with the number of sheets, supporting the reproducible and modular preparation method of CAT@NCF (Figure S10b, Supporting Information). Michaelis–Menten kinetics analysis for a sheet of CAT@NCF (d = 13 mm) gave a Michaelis–Menten constant (K_m) of 30.1 mM and the maximum reaction rate (V_{max}) of 1.71 µM sec^{-1} (Figures S13 and S14 and Table S4, Supporting Information). The reaction rate of CAT@NCF was lower than that of free CAT and the specific activity of CAT@NCF decreased following the increase of the total CAT loading amount (Figure S10c, Supporting Information), which can be ascribed to the restriction of substrate diffusion at the higher loading of CAT in the nanopores. Nonetheless, the maximum reaction rate per loaded CAT amount was comparable to the rate of CAT embedded in typical microporous framework

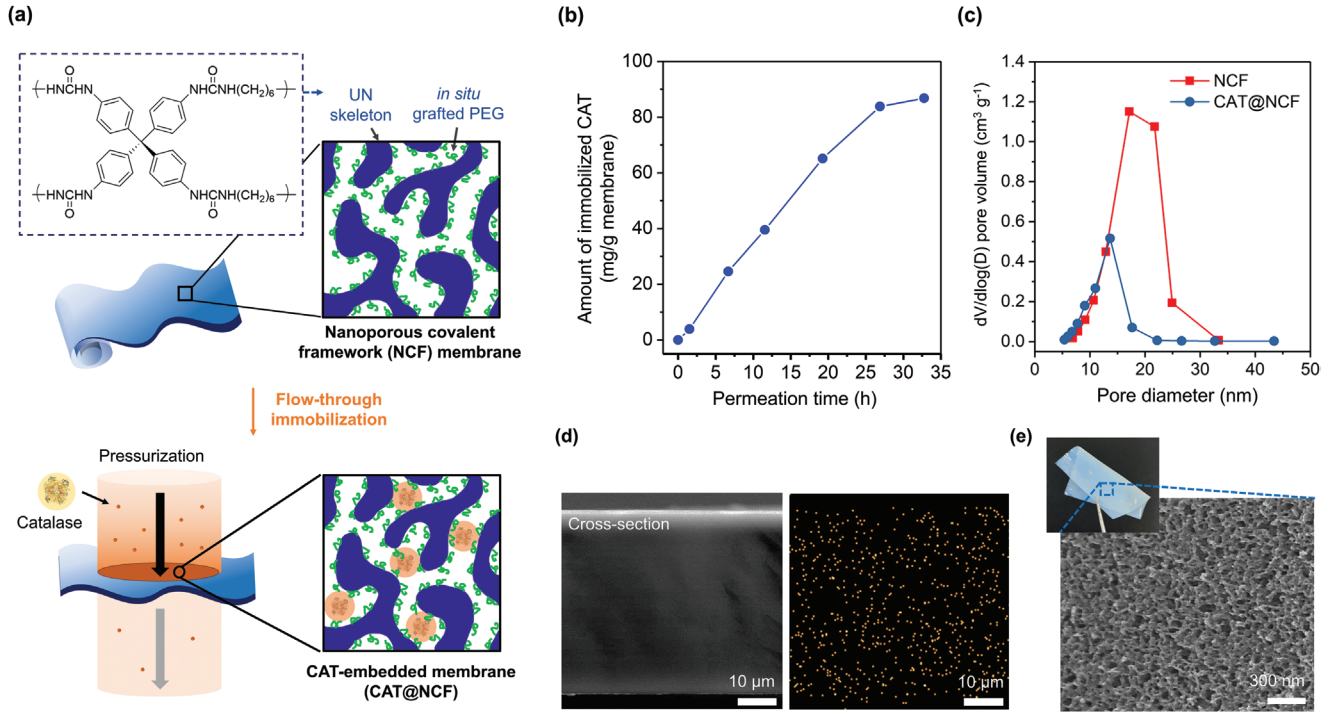

Figure 2. Synthetic procedure and pore structure of the catalase (CAT)-caged nanoporous covalent framework (NCF) membrane (CAT@NCF). a) Schematic illustration of the structure of the NCF membrane and the immobilization of CAT into the membrane. Pressure-driven flow-through permeation of the CAT solution enables dispersing CAT in the nanopores of NCF. b) The amount of the immobilized CAT as a function of permeation time. CAT feed solution was permeated through the membrane at 5 bar by nitrogen gas. The bicinchoninic acid assay was used to quantify CAT in the feed, permeate, and rinsing solution, from which the amount entrapped in the membrane was estimated (see Supporting Information for details). c) Barrett–Joyner–Halenda (BJH) pore size distribution of NCF and CAT@NCF obtained from nitrogen sorption experiments. d) A cross-sectional SEM image and SEM-EDX sulfur mapping of CAT@NCF. e) A magnified cross-sectional SEM image of CAT@NCF with the inset of a photograph of CAT@NCF film (3 cm × 3 cm).

materials but lower than that of CAT immobilized in macroporous materials (Table S5, Supporting Information).[50–58]

To ascertain the stability of CAT@NCF during repetitive reaction cycles, we carried out reuse experiments with a long duration of over 2.5 h. The membrane was removed with forceps, washed with a buffer solution, and put into a new batch of reactant solution. The CAT@NCF membrane catalyst maintained its activity during five cycles of reuse (Figure 3b;

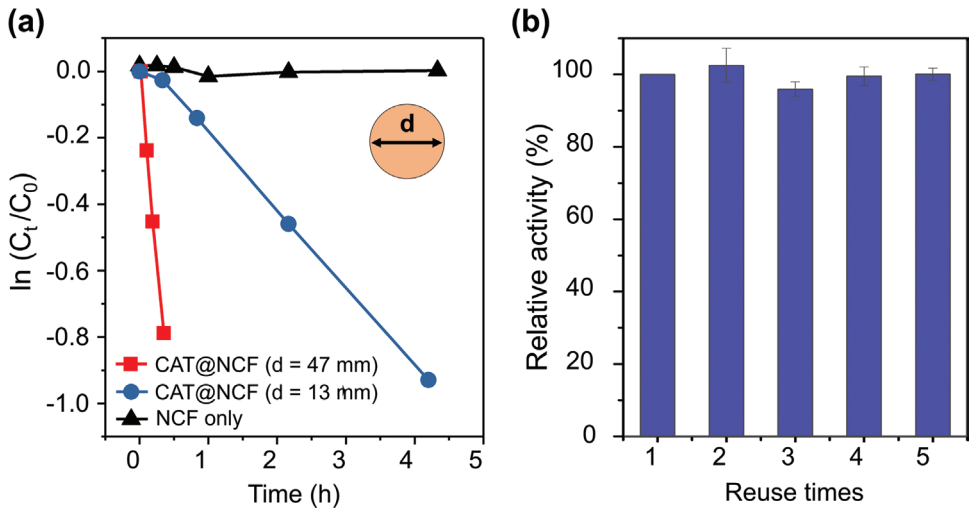

Figure 3. The activity of CAT@NCF membrane catalyst for hydrogen peroxide (H_2O_2) decomposition. a) Comparison of the activities of the CAT@NCF catalyst prepared from the different membrane sizes and the pristine NCF. C_t and C_0 represent the H_2O_2 concentration after reaction time (t) and the initial H_2O_2 concentration, respectively. b) The activity of the reused CAT@NCF at different times. CAT@NCF membrane was taken out by forceps, washed, and then put into a new batch of reactant solution.

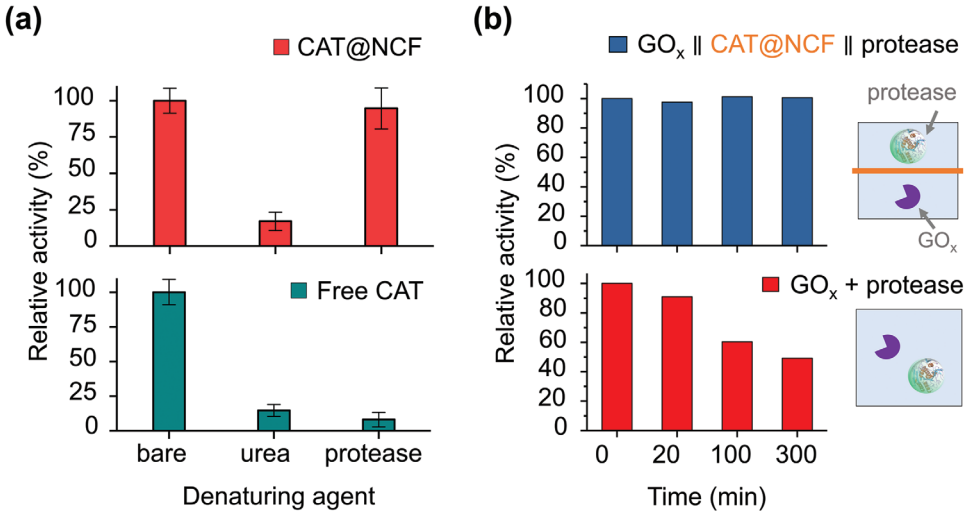

Figure 4. Size-exclusive shielding capacity of CAT@NCF bioactive film. a) H_2O_2 decomposition activity of CAT@NCF and free CAT after treatment with the deactivating agents (urea and protease). The activity was measured after the free CAT solution or the CAT@NCF-dipped solution was mixed with an aqueous urea solution of 12 M for 30 min and with a protease solution of 1 mg mL^{-1} for 2 h at room temperature, respectively. b) The activity after protease treatment of the GO_x enclosed in the CAT@NCF membrane compared with the solution without protection. The activity was monitored for different durations of protease treatment.

Figure S15, Supporting Information). The recycling procedure for CAT@NCF was more straightforward than other supported catalysts, which essentially require filtration or a repetitive centrifuge for recovery.[19,59] CAT@NCF was far more stable against thermal stress than free CAT. CAT@NCF maintained activity higher than 50% of the original activity above 60 °C, at which free CAT lost its activity nearly entirely. The 3D continuous nanopore of the NCF with a fixed range of pore size variation would protect the embedded CAT from the external deactivating agents greater than the sizes of the bottleneck pores. To prove this, we compared the activity of free CAT and CAT@NCF after exposure to protease (proteolytic agent) and urea (denaturing agent) (**Figure 4**a; Figure S16, Supporting Information). The hydrodynamic diameter of protease (≈4.2–5 nm)[60] was close to the smaller limit of the NCF pore size, whereas the molecular size of urea was 2.4 Å.[51] After protease treatment for 1 h (Figure 4a), the free CAT lost its activity to only 8.1% of the original value, but the CAT@NCF retained 98% of its activity. In contrast, urea treatment resulted in the loss of most activity of both free CAT and CAT@NCF. The result shows that the NCF pores protect their embedded enzyme from macromolecular inhibitors while allowing smaller molecular solutes to diffuse inside.

The CAT@NCF can protect another enzyme in its enclosed compartment (Figure 4b). We compared the activity of glucose oxidase (GO_x) in the presence or absence of the CAT@NCF barrier against a protease solution. The CAT@NCF spatially separated GO_x from the compartment containing protease. A homemade reaction container with an O-ring sealed membrane holder was set up to load a sheet of CAT@NCF. The facile thin film formulation of CAT@NCF enabled the construction of a compartmentalized platform. One side of CAT@NCF was open to a GO_x solution and the other was open to a protease solution The cell configuration was denoted as GO_x‖CAT@NCF‖protease for convenience). As a result, the activity of GO_x in the GO_x‖CAT@NCF‖protease remained intact. A control GO_x directly mixed with the protease solution decreased to almost half the initial activity after 5 h of incubation. The result shows that the NCF membranes are defect-free to prevent protease transport from the exterior into the inner compartment, which should enable more complex biocatalysis in the compartment of CAT@NCF barrier.

Last, we explored the potential of CAT@NCF to construct an artificial compartmentalized biocatalytic cascade system by taking advantage of the H_2O_2-scavenging/oxygen regeneration activity of CAT embedded in the membrane. We were inspired by the compartmentalized structure of peroxisome, in which the plasma membrane physically protects intracellular components and chemically detoxifies harmful compounds using its membrane-bound or soluble proteins (e.g., CAT) in the organelle.[7] We anticipated that the open and nanoporous structure of NCF would play a significant role similar to the cellular membrane, such as the transfer of small molecules and the blockage of large macromolecular denaturants, and that the embedded CAT would detoxify H_2O_2 and generate oxygen in the medium contacting CAT@NCF film.

The compartmentalized cascade reaction system of glucose oxidase (GO_x) and CAT@NCF was built, as shown in **Figure 5**a. A CAT@NCF membrane, held on a homemade holder, was contacted with a glucose/GO_x solution on one side of the membrane and an H_2O_2 solution on the other. GO_x oxidized glucose to gluconolactone, which was hydrolyzed to gluconic acid with the reduction of its flavin adenine dinucleotide (FAD) cofactor.[61,62] Oxygen was consumed to regenerate the cofactor by producing H_2O_2. H_2O_2 can deactivate GO_x when accumulated to high concentration; so, CAT is often used together to eliminate H_2O_2[63,64] and regenerate oxygen that can be further used for glucose oxidation by GO_x, closing the loop of a GO_x/CAT cascade.

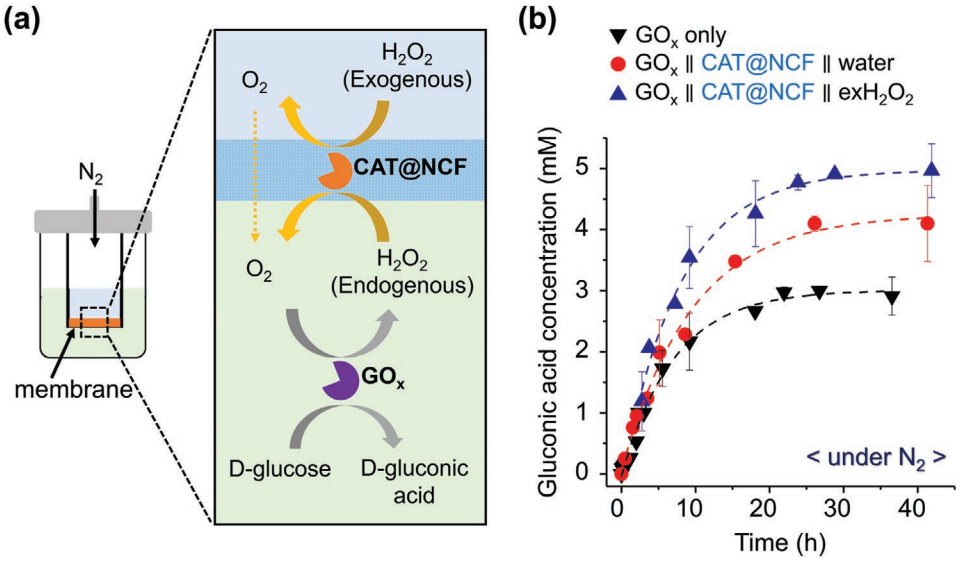

Figure 5. An artificial compartmentalized cascade reaction system with a CAT@NCF film and glucose oxidase (GO_x) under an anaerobic (nitrogen) environment. a) A membrane compartment was constructed by loading a CAT@NCF membrane in a homemade reaction container. The membrane interfaces glucose/GO_x solution on one side and H_2O_2 solution (or water) on the other. A cyclic cascade reaction of GO_x and CAT was mediated by hydrogen peroxide and oxygen. Endogenous H_2O_2 was generated from glucose oxidation by GO_x, and exogenous H_2O_2 (exH_2O_2) was supplied from the external compartment. b) Activity of GO_x in the absence of CAT@NCF or within CAT@NCF‖water or CAT@NCF‖exH_2O_2, respectively. For CAT@NCF‖exH_2O_2, a 10 mM exH_2O_2 solution was added to the upper compartment of CAT@NCF. The solution was degassed with nitrogen for 20 min, and the experiment was run under a nitrogen atmosphere. The gluconic acid concentrations at different reaction times were measured for the syringed liquid samples.

The activity of GO_x/CAT@NCF cascade was first monitored under anaerobic conditions (degassed and nitrogen gas-saturated reaction solution) to investigate the effect of reactive species (O_2 and H_2O_2) generated in situ by the CAT@NCF activity (Figure 5b). The initial activity of GO*x* was similar due to the O_2-independent intrinsic activity of GO_x until complete consumption of a cofactor (Figure S17, Supporting Information). A higher amount of gluconic acid was generated in the presence of CAT@NCF than without it. The endogenous H_2O_2 (enH_2O_2) generated from the GO_x activity was converted to oxygen by CAT@NCF at the interface and reused for glucose oxidation. However, it is noteworthy that CAT generates 1 mole of oxygen and 2 moles of water from 2 moles of H_2O_2, and that 1 mole of oxygen produces 1 mole of H_2O_2 in GO*x*-mediated glucose oxidation. In the closed oxygen/hydrogen peroxide redox loop, oxygen would be depleted without an external supply of H_2O_2 or oxygen to the system. The cascade reaction would eventually stop under anaerobic conditions as the initial supply of H_2O_2 and oxygen was depleted.

When an H_2O_2 (exH_2O_2) solution is added to the external compartment, CAT@NCF generates O_2 through the membrane to continue the GO_x activity. The highest amount of gluconic acid was generated by GO_x CAT@NCF‖exH_2O_2, where both enH_2O_2 and exH_2O_2 were employed to generate O_2. As the O_2 originating from the closed exH_2O_2 solution was also depleted over the multiple reaction cascades, the GO_x activity would stop because all types of oxygen sources are consumed entirely within the system.

In contrast to the anaerobic condition, GO_x within the CAT@NCF membrane under an air atmosphere (1 atm) (**Figure 6**a) continuously converted glucose into gluconic acid to a greater extent than in anaerobic conditions without reaching a plateau. As the oxygen from the internal GO*x* activity was negligible compared to a high external supply of oxygen from the air, both the GO*x* enclosed in the CAT@NCF and the free GO_x (without CAT@NCF) showed a similar production rate of gluconic acid over time (Figure S18, Supporting Information).

Essential functions of CAT@NCF arise when a high concentration of exH_2O_2 is provided in the outer solution of the membrane. At a concentration of exH_2O_2 higher than a several-milli-molar range (Figure 6a), GO_x‖CAT@NCF‖exH_2O_2 shows higher activity than GO_x‖CAT@NCF‖water for a prolonged time. It is known that the oxygen solubility in water (≈0.2 mM at 35 °C) is relatively low compared to the Michaelis–Menten constant of GO_x for O_2 (K_{MO} = 0.51 mM).[65] The enhanced reaction rate in GO_x‖CAT@NCF‖exH_2O_2 suggests that the CAT@NCF with exH_2O_2 supplies oxygen more rapidly than the direct dissolution of oxygen from the air. exH_2O_2 diffuses through the CAT@NCF membrane owing to its high concentration gradient across the membrane between two compartments, during which it transforms into oxygen. The degree of oxidation reaction can be controlled by the concentration of exH_2O_2, as shown in Figure 6b, in which the concentration of the generated gluconic acid increases linearly with the concentration of exH_2O_2 provided from the outer compartment.

A different role of the CAT@NCF membrane is protecting the enzymes in the inner compartment from damage by a high exH_2O_2 concentration. In Figure 6a, in the presence of exH_2O_2, the GO_x enclosed in NCF without CAT (black square) shows much lower activity than in the CAT@NCF (blue circle). GO*x* is deactivated seriously in the absence of CAT in the NCF because of the diffusion of exH_2O_2 (Figure S19, Supporting

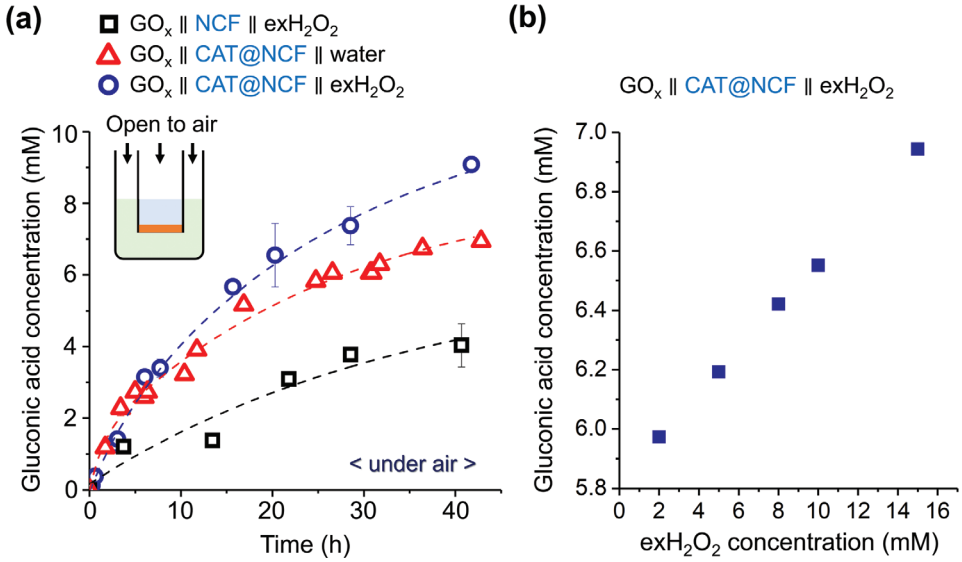

Figure 6. Demonstration of the enhanced cascade reaction of glucose oxidase (GO_x) and CAT and the bioactive protection by CAT@NCF film under an air atmosphere (1 atm). a) Activity of GO_x in the presence of CAT@NCF membrane with (circle) or without (triangle) external H_2O_2 supply as compared with the absence of CAT@NCF membrane with external H_2O_2 supply (square). The reaction container was open to air during the oxidation reaction. Deionized water or 10 mM exogenous H_2O_2 (exH_2O_2) aqueous solution was added to the upper compartment of CAT@NCF. b) GO_x activity in the compartment GO_x‖CAT@NCF‖exH_2O_2 with different concentrations of exH_2O_2 in the upper compartment. The gluconic acid concentration was measured after 20 h of GO_x reaction.

Information). Integrating CAT in NCF can effectively protect GO_x inside the compartment from oxidative stress, enabling the cascade reaction to continue for a prolonged time. Furthermore, as expected from the experiment shown above (Figure 4b), the CAT@NCF helped maintain the GO_x activity when a protease solution was added to the outer compartment (Figure S20, Supporting Information).

The overall results demonstrate the CAT@NCF as an active barrier for constructing artificial biological compartments by protecting the encapsulated species physically and chemically from an external environment. This is the first report on a macroscale artificial compartmentalized biocatalytic cascade reactor connected by the mesopore-confined enzymes to the external medium. The potential applications of the cascade reaction system are numerous, including its incorporation into biohybrid devices that contain tissues and cells. For example, it could be used to create a controllable oxygen-generation film that utilizes external hydrogen peroxide sources to aid in wound healing or an interfacial membrane support that regulates cell growth in organ-on-a-chip devices. It is also possible to create multi-compartment biocatalytic systems that mimic tissue-like functionalities by stacking multiple sheets of enzyme@NCF films, thanks to the simple enzyme immobilization method.

3. Conclusion

We have demonstrated an artificial compartmentalized biochemical cascade system by CAT embedded in the reticulated nanochannels of the NCF membrane. The CAT@NCF film showed prolonged biocatalytic activity and size-exclusive protection due to the nanopores while allowing molecular transport. A compartmentalized architecture with a cascade reaction of GO_x/CAT@NCF showed multiple bioactive capabilities and barrier properties, including hydrogen peroxide detoxification, in situ oxygen generation, and protease exclusion. We expect such enzyme-embedded biocatalytic membrane scaffolds can be applied to other enzymatic cascade reactions. The synthetic scalability and post-shaping capability are promising aspects for adopting the Enzyme@NCF into biohybrid devices such as soft robots and sensors.

4. Experimental Section

Materials and Methods: Tetrakis(4-aminophenyl) methane (TAPM) was synthesized as previously reported with modification.[66] Hexamethylene diisocyanate (HDI) (99%, Sigma–Aldrich) was freshly distilled under reduced pressure. Anhydrous grade solvents of *N*,*N*-dimethylformamide (DMF) (99.8%) were purchased from Sigma–Aldrich. Poly (ethylene glycol) (PEG) (PEG35000) was purchased from Sigma–Aldrich. The weight average molecular weight (M_w) and number average molecular weight (M_n) of PEG were obtained by gel permeation chromatography (GPC) (M_w = 31 100 Da and M_n = 27 100 Da). The polymer was used after drying at least for 24 h in a desiccator before use. Catalase from bovine liver (CAT), bovine serum albumin (BSA), protease from *Streptomyces griseus* (Type XIV, ≥3.5 units per mg), and Proteinase K from *Tritirachium album* were purchased from Sigma–Aldrich and used without further purification. Hydrogen peroxide (30%) and urea were purchased from Sigma–Aldrich. Tetrahydrofuran (THF) (99.9%) was purchased from commercial sources and used without further purification. Pierce Quantitative Peroxide Assay Kits were purchased from Thermo Scientific.

Characterization: Scanning electron microscopy (SEM) was performed on a Hitachi/S-4700 field emission scanning electron microscope. Sample films for cross-section analysis were fractured in liquid nitrogen and dried at 100 °C for 24 h under vacuum. The samples were then coated with 3 nm of platinum using sputter before SEM imaging. Elemental mapping was conducted by energy dispersive X-ray spectrometry (EDX) coupled with the SEM equipment. The fourier transform infrared (FTIR) spectra (4000–400 cm^{-1}) were recorded by a System 2000 FTIR

spectrophotometer (Perkin Elmer). FTIR samples of polymers were prepared by the KBr pellet method, and free-standing films of PEG/UN blend, NCF, and CAT@NCF were used for measurements. The molecular weights of PEGs were obtained with the three columns (two TSKgel GMPWxl and TSKgel G2500PWxl [7.8×300 mm]) and a Tskgel guard PWxl guard column. 0.1 M $NaNO_3$ aqueous solution was used as eluent with a flow rate of 1.0 mL min^{-1} at 40 °C. A calibration curve was obtained using monodisperse PEG as a standard. Gas sorption isotherms were obtained from ASAP 2020 accelerated surface area and porosimetry system (Micromeritics, USA) within a range of relative pressure from 0.0 to 1.0 for nitrogen at 77K. The samples were separately degassed in a degas port of the analyzer at 423 K for at least 12 h prior to analysis. The Brunauer–Emmett–Teller (BET) surface area, pore volume, and Barrett–Joyner–Halenda (BJH) pore size distribution were obtained using ASAP 2020 ver 3.00 software.

Preparation of Urea-Bonded Network (UN) Sols: A 0.04 g mL^{-1} UN sol was prepared by the previously reported method.[34] In brief, tetrakis (4-aminopheyl) methane (TAPM) (0.200 g, 0.526 mmol) was dissolved in 5 mL of anhydrous DMF in a round-bottom Schlenk flask under a nitrogen atmosphere. The solution was added to a solution of distilled hexamethylene diisocyanate (HDI) (0.175 g, 1.052 mmol) in DMF (4.4 mL) at room temperature. The reaction mixture remained in the liquid sol state until the gelation time (t_g), which was ≈85 h for a concentration of 0.04 g mL^{-1}.

A Typical Procedure for Preparation of Nanoporous Covalent Framework (NCF) Membrane: In a typical UN sol preparation for blending with PEG, UN monomer solution mixture was kept for 60 h at room temperature. PEG was added to the UN sol prepared from the above. The weight fraction of PEG relative to UN sol (W_p) was kept as 0.6. The PEG/UN sol mixture was heated at 50 °C and stirred for 2 h. The solution was cooled to room temperature for 30 min under stirring after removing the heating bath. The resulting PEG/UN sol mixture was cast onto a glass plate, and the solvent was evaporated by heating sequentially at the designated temperatures under nitrogen flow. The temperature increasing rate was 1 °C min^{-1}. After solvent evaporation, the glass plate with the film was immersed in water to obtain free-standing PEG/UN blend film, which was then kept for 7 days to remove PEG from the blend film.

Permeation Properties of NCF Membrane: The flux of solvents through the NCF membrane was measured using a dead-end filtration stirred cell (Sterlitech HP4750 stirred cell; Kent, USA) with a home-made membrane holder accessory for smaller membrane size (diameter = 13 mm). The effective surface area of the membrane for permeation was 6.4×10^{-5} m^2. The membrane cell was connected to a nitrogen gas cylinder (99.999%) equipped with a pressure regulator. The cell was pressurized using nitrogen gas at 5 bar. As-synthesized NCF membranes were dipped in water for at least 1 h before the permeation experiment. The time-dependent solvent flux of the membrane was determined by measuring volumetric flux typically at 5 bar. The solvent permeation flux (J) of NCF membrane was calculated as follows:

$$J = \frac{V}{A \times \Delta t} \quad (1)$$

where J (L m^{-2} h^{-1}) is the solvent permeation flux, V (L) is the volume of the permeate, A (m^2) is the effective membrane area, and Δt (h) is the permeation time.

Preparation of CAT@NCF Membrane Catalyst by Permeation of CAT Feed Solution: Catalase (CAT) solution was prepared by adding 3 mg of CAT into 100 mL of phosphate buffer solution (5 mM and pH 7.4) and stirring for 30 min at room temperature. The solution was filtered with a cellulose acetate syringe filter (pore diameter = 0.2 µm). The feed solution was permeated through NCF membrane by applying nitrogen gas at 5 bar at room temperature. The typical permeation time for CAT immobilization was 24 h. The CAT@NCF film was stored in a phosphate buffer (5 mM and pH 7.4) at 4 °C. The amount of immobilized CAT was estimated using bicinchoninic acid (BCA) assay with UV/Vis spectrometer (The detailed procedure is given in Supporting Information). Solutions of Bovine Serum Albumin with different concentrations were used to obtain a standard curve. The manufacturer's protocol was followed with a slight modification.

Catalytic Decomposition of H_2O_2 by Free CAT and CAT@NCF Membrane Catalyst: Hydrogen peroxide stock solution (30%) was diluted with deionized water to obtain ≈0.1–10 mM substrate solutions. Free CAT solution was prepared by dissolving CAT in 5 mL of 10 mM phosphate buffer to obtain 1 mg L^{-1}. 5 mL of diluted H_2O_2 solution was added to the CAT solution and stirred at room temperature. In typical experiments, a sheet of CAT@NCF membrane was dipped in 5 mL of phosphate buffer solution (10 mM, pH = 7.4). To the solution, was added 5 mL of H_2O_2 solution. The concentration of H_2O_2 was monitored by UV/Vis spectrometer (λ_{max} = 240 nm). Reference experiments with NCF membranes and multiple sheets of CAT@NCF membranes were conducted similarly. To perform an assay of H_2O_2 solution of concentration lower than 0.1 mM, ferrous Oxidation in Xylenol orange (FOX) assay was conducted with a protocol modified for this study. In brief, 30 µL of H_2O_2 standard solution at various concentrations (or sample solutions) was diluted with 1260 µL of deionized water. Then, the solution was mixed with 600 µL of FOX reagent solution and incubated for 1 h 30 min at room temperature to ensure complete reaction. The FOX reagent solution was prepared by mixing reagent A (composed of 25 mM ammonium ferrous (II) sulfate and 2.5 M H_2SO_4) and reagent B (125 µM xylenol orange and 100 mM sorbitol). Absorbance at 560 nm was read by UV/Vis spectrometer with a quartz cuvette.

Repeated Use Experiment of CAT@NCF Membrane Catalyst: Activity of CAT@NCF at 1 mM of H_2O_2 solution was tested using the method mentioned above. After 30 min of reaction, the CAT@NCF was taken out from the solution by forceps and washed with 5 mM phosphate buffer (pH = 7.4). Then, the membrane catalyst was dipped in another batch solution of H_2O_2. The activity measurement was repeated five times.

Effect of Preheating Temperature on the Activity of CAT@NCF and Free CAT: Free CAT solution and CAT@NCF dipped in buffer solution were prepared following the typical procedure mentioned above. The solutions were heated at the designated temperatures (≈25–70 °C) for 30 min and cooled to room temperature prior to the activity measurements. Activity assay was performed by FOX assay using the typical method.

Protease Treatment of Free CAT and CAT@NCF Membrane Catalyst: 1 mg mL^{-1} protease solution was prepared by dissolving 0.005 g of protease in 5 mL of 10 mM phosphate buffer solution (pH = 7.4). A sheet of CAT@NCF was incubated in 2.5 mL of 10 mM phosphate buffer for 10 min. To the CAT@NCF solution and 2.5 mL of 1 mg L^{-1} free CAT solution, was added 2.5 mL of the protease solution, and then kept for 2 h at room temperature. 5 mL of 0.2 mM H_2O_2 solution was added to the solution. The activity of CAT or CAT@NCF was assayed in the presence of protease by FOX assay as mentioned above.

Urea Denaturant Treatment of Free CAT and CAT@NCF Membrane Catalyst: 12 M urea solution was prepared in 10 mM phosphate buffer solution (pH = 7.4). To 2.5 mL of CAT@NCF solution or 1 mg L^{-1} free CAT solution was added, 2.5 mL of urea solution, then kept for 30 min at room temperature. 5 mL of 0.2 mM H_2O_2 solution was added to the mixture and the concentration of the remaining H_2O_2 was monitored by FOX assay.

Demonstration of Dual Protection of CAT@NCF Against H_2O_2 and Protease: A homemade membrane holder connected to a disposable polypropylene syringe barrel was used for loading solution of deactivation agent (H_2O_2 and protease) and allowing diffusion through the membrane. The holder was placed in a larger vessel that formed the outer compartment, while the syringe barrel formed the inner compartment. Membranes (commercial cellulose acetate membrane with a pore diameter of 0.45 µm, NCF membrane, and CAT@NCF membrane) were loaded in a membrane holder that was tightly sealed by an O-ring. The outer solution was stirred to minimize the unstirred water layer effect. H_2O_2 scavenging capability was assessed by the following procedure. 5 mL of 30 mg L^{-1} glucose oxidase (GO_x) solution in deionized water was added into the outer compartment. 5 mL of 10 mM H_2O_2 solution was added to the inner compartment, and the set-up was kept for 1 h at room temperature. The reference experiment without membrane was done by directly mixing H_2O_2 solution with GO_x

solution. The temperature of the reactor was set to 35 °C, and 20 mL of 200 mM glucose solution was then added to the outer compartment. The concentration of gluconic acid was monitored by a back titration method. 0.2 mL of sample aliquot was mixed with 0.4 mL of 80 mM NaOH solution and titrated with 10 mM HCl using a micro burette. The protease-resistant capability was assessed by a method similar to the above procedure using protease solution instead of H_2O_2. 5 mL of 0.4 mg mL^{-1} of Proteinase K solution was prepared in deionized water and added into the inner compartment of the reactor. The temperature of the reactor was kept at 40 °C for 1 h. The activity of GO_x was monitored by the method described above.

Supporting Information

Supporting Information is available from the Wiley Online Library or from the author.

Acknowledgements

This research was supported by the National Research Foundation of Korea (NRF) grant funded by the Korean government (NRF-2021R1A2C2011530).

Conflict of Interest

The authors declare no conflict of interest.

Data Availability Statement

The data that support the findings of this study are available from the corresponding author upon reasonable request.

Keywords

compartmentalization, enzyme cascade, enzyme immobilization, mesoporous materials, nanoporous membrane

Received: March 4, 2023
Revised: April 15, 2023
Published online: May 15, 2023

[1] M. Miller, M. Hafner, E. Sontag, N. Davidsohn, S. Subramanian, P. E. M. Purnick, D. Lauffenburger, R. Weiss, *PLoS Comput. Biol.* **2012**, *8*, e1002579.
[2] Y. Yang, X. Zhao, J. Yu, X. Chen, R. Wang, M. Zhang, Q. Zhang, Y. Zhang, S. Wang, Y. Cheng, *Bioact. Mater.* **2021**, *6*, 3962.
[3] M. Marguet, C. Bonduelle, S. Lecommandoux, *Chem. Soc. Rev.* **2012**, *42*, 512.
[4] Y. Shen, P. O. Saboe, I. T. Sines, M. Erbakan, M. Kumar, *J. Membr. Sci.* **2014**, *454*, 359.
[5] S. Wu, A. Buthe, H. Jia, M. Zhang, M. Ishii, P. Wang, *Biotechnol. Bioeng.* **2013**, *110*, 1805.
[6] D. Moreira, B. Gullón, P. Gullón, A. Gomes, F. Tavaria, *Food Funct.* **2016**, *7*, 3273.
[7] A. G. Grigoras, *Biochem. Eng. J.* **2017**, *117*, 1.
[8] M. Sára, U. B. Sleytr, *Prog. Biophys. Mol. Biol.* **1996**, *65*, 83.
[9] T. Pols, H. R. Sikkema, B. F. Gaastra, J. Frallicciardi, W. M. Śmigiel, S. Singh, B. Poolman, *Nat. Commun.* **2019**, *10*, 4239.
[10] B. C. Buddingh', J. C. M. van Hest, *Acc. Chem. Res.* **2017**, *50*, 769.
[11] T. Heuser, E. Weyandt, A. Walther, *Angew. Chem., Int. Ed.* **2015**, *54*, 13258.
[12] A. H. Chen, P. A. Silver, *Trends Cell Biol.* **2012**, *22*, 662.
[13] D. M. Vriezema, P. M. L. Garcia, N. Sancho Oltra, N. S. Hatzakis, S. M. Kuiper, R. J. M. Nolte, A. E. Rowan, J. C. M. van Hest, *Angew. Chem., Int. Ed.* **2007**, *46*, 7378.
[14] H.-C. Chiu, Y.-W. Lin, Y.-F. Huang, C.-K. Chuang, C.-S. Chern, *Angew. Chem., Int. Ed.* **2008**, *47*, 1875.
[15] I. C. Lopes, A. Zebda, P. Vadgama, *Curr. Opin. Electrochem.* **2018**, *12*, 107.
[16] A. Economou, C. Kokkinos, M. Prodromidis, *Lab Chip* **2018**, *18*, 1812.
[17] L. Ouyang, J. P. K. Armstrong, M. Salmeron-Sanchez, M. M. Stevens, *Adv. Funct. Mater.* **2020**, *30*, 1909009.
[18] G. Villar, A. D. Graham, H. Bayley, *Science* **2013**, *340*, 48.
[19] P. Wied, F. Carraro, J. M. Bolivar, C. J. Doonan, P. Falcaro, B. Nidetzky, *Angew. Chem., Int. Ed.* **2022**, *61*, e202117345.
[20] H. An, J. Song, T. Wang, N. Xiao, Z. Zhang, P. Cheng, S. Ma, H. Huang, Y. Chen, *Angew. Chem., Int. Ed.* **2020**, *59*, 16764.
[21] K. O. Ramberg, S. Engilberge, T. Skorek, P. B. Crowley, *J. Am. Chem. Soc.* **2021**, *143*, 1896.
[22] Y. Chen, P. Li, J. Zhou, C. T. Buru, L. Đorđević, P. Li, X. Zhang, M. M. Cetin, J. F. Stoddart, S. I. Stupp, M. R. Wasielewski, O. K. Farha, *J. Am. Chem. Soc.* **2020**, *142*, 1768.
[23] H.-J. Choi, C. D. Montemagno, *Nano Lett.* **2005**, *5*, 2538.
[24] X. Huang, M. Li, S. Mann, *Chem. Commun.* **2014**, *50*, 6278.
[25] M. de J. Velásquez-Hernández, E. Astria, S. Winkler, W. Liang, H. Wiltsche, A. Poddar, R. Shukla, G. Prestwich, J. Paderi, P. Salcedo-Abraira, H. Amenitsch, P. Horcajada, C. J. Doonan, P. Falcaro, *Chem. Sci.* **2020**, *11*, 10835.
[26] S. Huang, G. Chen, G. Ouyang, *Chem. Soc. Rev.* **2022**, *51*, 6824.
[27] P. Zhang, A. Fischer, Y. Ouyang, J. Wang, Y. S. Sohn, O. Karmi, R. Nechushtai, I. Willner, *Chem. Sci.* **2022**, *13*, 7437.
[28] K. Hemmer, M. Cokoja, R. A. Fischer, *ChemCatChem* **2021**, *13*, 1683.
[29] L. D. Blackman, S. Varlas, M. C. Arno, Z. H. Houston, N. L. Fletcher, K. J. Thurecht, M. Hasan, M. I. Gibson, R. K. O'Reilly, *ACS Cent. Sci.* **2018**, *4*, 718.
[30] E. Serebryany, G. A. Zhu, E. C. Y. Yan, *Biochim. Biophys. Acta, Biomembr.* **2012**, *1818*, 225.
[31] Y. Xu, J. Fei, G. Li, T. Yuan, J. Li, *ACS Nano* **2017**, *11*, 10175.
[32] C. H. Nielsen, *Anal. Bioanal. Chem.* **2009**, *395*, 697.
[33] R. Mazzei, A. Yihdego Gebreyohannes, E. Papaioannou, S. P. Nunes, I. F. J. Vankelecom, L. Giorno, *Bioresour. Technol.* **2021**, *335*, 125248.
[34] S.-Y. Moon, J.-S. Bae, E. Jeon, J.-W. Park, *Angew. Chem., Int. Ed.* **2010**, *49*, 9504.
[35] J.-S. Bae, E. Jeon, S.-Y. Moon, W. Oh, S.-Y. Han, J. H. Lee, S. Y. Yang, D.-M. Kim, J.-W. Park, *Angew. Chem., Int. Ed.* **2016**, *55*, 11495.
[36] W. Oh, J.-W. Park, *ACS Appl. Mater. Interfaces* **2019**, *11*, 32398.
[37] W. Oh, G.-B. Lee, D. Jeong, J.-W. Park, *J. Membr. Sci.* **2023**, *669*, 121341.
[38] B. Panganiban, B. Qiao, T. Jiang, C. DelRe, M. M. Obadia, T. D. Nguyen, A. A. A. Smith, A. Hall, I. Sit, M. G. Crosby, P. B. Dennis, E. Drockenmuller, M. Olvera de la Cruz, T. Xu, *Science* **2018**, *359*, 1239.
[39] J. Fu, R. B. Schoch, A. L. Stevens, S. R. Tannenbaum, J. Han, *Nat. Nanotechnol.* **2007**, *2*, 121.
[40] L. Liu, P. Li, S. A. Asher, *Nature* **1999**, *397*, 141.
[41] F. Zhang, M. Wang, C. Liang, H. Jiang, J. Shen, H. Li, *Sci. Rep.* **2014**, *4*, 4421.
[42] J. Luo, F. Marpani, R. Brites, L. Frederiksen, A. S. Meyer, G. Jonsson, M. Pinelo, *J. Membr. Sci.* **2014**, *459*, 1.
[43] J. Luo, A. S. Meyer, G. Jonsson, M. Pinelo, *Bioresour. Technol.* **2013**, *147*, 260.

[44] I. Fita, M. G. Rossmann, *Proc. Natl. Acad. Sci. U. S. A.* **1985**, *82*, 1604.
[45] W. Oh, J.-S. Bae, J.-W. Park, *Macromolecules* **2021**, *54*, 1192.
[46] C. Lei, Y. Shin, J. Liu, E. J. Ackerman, *J. Am. Chem. Soc.* **2002**, *124*, 11242.
[47] B. Chen, E. M. Miller, L. Miller, J. J. Maikner, R. A. Gross, *Langmuir* **2007**, *23*, 1381.
[48] D. Usoltsev, V. Sitnikova, A. Kajava, M. Uspenskaya, *Biomolecules* **2019**, *9*, 359.
[49] J. Kong, S. Yu, *Acta Biochim. Biophys. Sin.* **2007**, *39*, 549.
[50] F.-K. Shieh, S.-C. Wang, C.-I. Yen, C.-C. Wu, S. Dutta, L.-Y. Chou, J. V. Morabito, P. Hu, M.-H. Hsu, K. C.-W. Wu, C.-K. Tsung, *J. Am. Chem. Soc.* **2015**, *137*, 4276.
[51] F.-S. Liao, W.-S. Lo, Y.-S. Hsu, C.-C. Wu, S.-C. Wang, F.-K. Shieh, J. V. Morabito, L.-Y. Chou, K. C.-W. Wu, C.-K. Tsung, *J. Am. Chem. Soc.* **2017**, *139*, 6530.
[52] J. Cui, Y. Feng, S. Jia, *Chem. Eng. J.* **2018**, *351*, 506.
[53] T.-H. Wei, S.-H. Wu, Y.-D. Huang, W.-S. Lo, B. P. Williams, S.-Y. Chen, H.-C. Yang, Y.-S. Hsu, Z.-Y. Lin, X.-H. Chen, P.-E. Kuo, L.-Y. Chou, C.-K. Tsung, F.-K. Shieh, *Nat. Commun.* **2019**, *10*, 5002.
[54] W. Liang, F. Carraro, M. B. Solomon, S. G. Bell, H. Amenitsch, C. J. Sumby, N. G. White, P. Falcaro, C. J. Doonan, *J. Am. Chem. Soc.* **2019**, *141*, 14298.
[55] M. Li, S. Qiao, Y. Zheng, Y. H. Andaloussi, X. Li, Z. Zhang, A. Li, P. Cheng, S. Ma, Y. Chen, *J. Am. Chem. Soc.* **2020**, *142*, 6675.
[56] Ş. Akkuş Çetinus, H. N. Öztop, *Enzyme Microb. Technol.* **2000**, *26*, 497.
[57] A. M. Eberhardt, V. Pedroni, M. Volpe, M. L. Ferreira, *Appl. Catal., B* **2004**, *47*, 153.
[58] N. Misra, N. K. Goel, S. A. Shelkar, L. Varshney, V. Kumar, *J. Mol. Catal. B: Enzym.* **2016**, *133*, S172.
[59] A. M. García-Campaña, *Chemiluminescence in Analytical Chemistry*, 1st ed., CRC Press, Boca Raton, FL **2001**.
[60] P. J. Sweeney, J. M. Walker, in *Enzymes of Molecular Biology* (Ed: M. M. Burrel), Humana Press, Totowa, NJ **1993**, p. 271.
[61] J. F. Kornecki, D. Carballares, P. W. Tardioli, R. C. Rodrigues, Á. Berenguer-Murcia, A. R. Alcántara, R. Fernandez-Lafuente, *Catal. Sci. Technol.* **2020**, *10*, 5740.
[62] V. Leskovac, S. Trivić, G. Wohlfahrt, J. Kandrač, D. Peričin, *Int. J. Biochem. Cell Biol.* **2005**, *37*, 731.
[63] L. Vermeiren, F. Devlieghere, M. van Beest, N. de Kruijf, J. Debevere, *Trends Food Sci. Technol.* **1999**, *10*, 77.
[64] T. Godjevargova, R. Dayal, I. Marinov, *J. Appl. Polym. Sci.* **2004**, *91*, 4057.
[65] R. M. Lindeque, J. M. Woodley, *Org. Process Res. Dev.* **2020**, *24*, 2055.
[66] P. Ganesan, X. Yang, J. Loos, T. J. Savenije, R. D. Abellon, H. Zuilhof, E. J. R. Sudhölter, *J. Am. Chem. Soc.* **2005**, *127*, 14530.